AIAA JOURNAL
Vol. 36, No. 11, November 1998

Mixing Enhancement in High-Speed Turbulent Shear Layers Using Excited Coherent Modes

K. Lee* and J. T. C. Liu†
Brown University, Providence, Rhode Island 02912-9104

For noise reduction purposes, it is often desirable to promote rapid mixing close to the jet exhaust. Excited high-frequency coherent wave modes for mixing enhancement in the initial region of high-speed jet exhaust were studied theoretically. The jet in this region is modeled as a two-dimensional mixing layer. Integral kinetic energy equations for the mean flow and the control modes are derived from the compressible Navier–Stokes equations, with the flow quantities split into mean, coherent wave modes and fine-grained turbulence. Turbulence effects are characterized by an eddy viscosity; the coherent modes are explicitly characterized by their nonlinear amplitudes and the shape functions of the eigenmodes of a local linear stability theory according to the developing shear layer. The initial region considered is two dimensional where the initial boundary layer is assumed to be thin relative to the jet size. The upstream velocity and temperature wake, due to wall boundary layers, are accommodated in the mean flow shape assumptions. Two significant nonequilibrium effects associated with the initial control region are 1) the imbedded wake evolves into a similar mixing region downstream and 2) the interaction between excited control modes and the mean flow is strongly dependent on initial conditions. It is found that excitation of high-frequency modes could give rise to enhanced spreading of the mixing layer in the initial wake mixing-layer region; the effects of varying the relative initial two stream shear-layer thickness and temperature ratios are also studied.

Nomenclature

A = coherent mode amplitude function
c = complex phase velocity
c_p = heat capacity at constant pressure
F = shape function of u'
H = mean total enthalpy
I_{ke} = coherent mode kinetic energy advection integral
I_M, I_Φ = mean flow kinetic energy-defect advection and turbulent dissipation
I_p = pressure work integral
I_{rs} = Reynolds stress-energy conversion integral
I_ϕ = turbulent dissipation integral
I_1, I_2 = momentum integrals
M = Mach number
M_c = convection Mach number
P = wake function; Eq. (5)
R = shape function of ρ'
R_T = turbulent Reynolds number
r = proportionality constant in u_{cw}
T = temperature
t = time
U = undisturbed stream velocity
u, v = streamwise, normal velocity components
x, y = streamwise, normal coordinates
α = streamwise wave number
$\alpha\phi$ = shape function of v'
β = undisturbed stream velocity, total enthalpy, temperature ratios
γ = ratio of specific heats
η = transformed similarity variable
θ = momentum thickness
ξ = $x - x_0$
π = shape function of p'
ρ = density
ω = frequency

Subscripts

cm = centerline value of mixing-layer profile contribution
cw = centerline value of wake profile contribution
i = imaginary part
m = mixing-layer profile contribution
r = real part; reference value
w = wake profile contribution
0 = upstream, initial values
1 = hot core region ($y > 0$)
2 = cooler, external stream ($y < 0$)

Superscripts

$\bar{}$ = time-averaged mean
$'$ = control mode quantities; differentiation with respect to η
$*$ = centerline value
$\tilde{}$ = incompressible

Presented as Paper 96-0547 at the AIAA 34th Aerospace Sciences Meeting, Reno, NV, Jan. 15–19, 1996; received July 5, 1997; revision received July 20, 1998; accepted for publication July 21, 1998.

Dedicated to the memory of Sir James Lighthill, 1924–1998.

*Postdoctoral Research Associate, Division of Engineering.
†Professor of Engineering, Division of Engineering and the Center for Fluid Mechanics, Turbulence, and Computation. Associate Fellow AIAA.

I. Introduction

On the basis of experimental evidence, it is now well known that noise sources are located far downstream from the jet nozzle exit and in the vicinity of the end of the potential core region.[1–4] The observation of distinct large-scale coherent structures in the mixing layer by Brown and Roshko[5–7] stimulated the modeling of noise sources as streamwise developing instability waves in a high-speed developing shear layer[8,9] and two-dimensional supersonic jet,[10] as well as high- and low-speed round jets.[11,12] As such, the amplitude of each frequency component peaks farther downstream with decreasing frequency until the end of the potential core region, where the well-mixed developed jet region causes more severe damping of the coherent structure energy and the cutoff of energy supply from the weakened mean flow.[10] Such model computations were able to produce sound pressure levels in the near jet noise field for supersonic two-dimensional jets[10] and round jets[11] that bear strong resemblance to near-field measurements in pattern and in decibel levels. In fact, modeled noise sources[12] in a low-speed round jet gave a far sound field computed from Lighthill's integral that is amazingly close to observations[13,14] in terms of frequency-dependent

directivity. We refer to Mankbadi et al.[15] and Bastin et al.[16] for discussions of computational issues in modeling developing large-scale wave-like eddies as noise sources[9,10] and their far aerodynamic sound field.

For an undisturbed high-speed jet, the end of the potential core is some 10 diameters downstream at an exit Mach number of about two, e.g., see Ref. 17. It is known from theoretical studies in low-speed flow, e.g., see Ref. 18, as well as experimental studies[19,20] that excited coherent modes at the correct frequency range and at sufficient amplitudes could alter the mean flow, which in turn modifies the development of all other unforced modes.

Our objective is to show that mixing between a high-speed, hot jet exhaust and slower speed, cooler air could be enhanced via excitation of coherent instabilities inherently present in the flow within an initial frequency and amplitude range. This is accomplished through use of approximate methods with rapid estimation possibilities over parameter space. For practical noise abatement reasons, the mixing enhancement must necessarily take place in the initial region of the jet exhaust rather than in the far downstream similarity region. In this case, the initial region is well approximated as a two-dimensional mixing layer supporting the developing wave-like eddies as noise sources discussed by Liu.[9] The use of control modes in this initial region will bring on two distinct nonequilibrium effects. 1) One is the adjustment of the mean flow wake-like velocity and temperature profiles, set up by upstream wall boundary layers, toward the similarity profiles downstream. 2) The other is the nonequilibrium interaction between the control modes and the mean flow. The mean flow adjustment is hastened through the use of control modes, and this can be optimally accomplished through the use of wake shear-layer modes, which are at frequencies considerably higher than the dominant noise-producing jet modes. In this study, only two-dimensional modes are used, which forms the basis for extension to three-dimensional modes. The two-dimensional modes are essentially axisymmetric modes in the initial region of a round jet exhaust, where the exit boundary-layer thickness is much smaller than the jet nozzle radius.

The plan of the paper is as follows. The general formulation is first discussed in Sec. II, the derivation of the nonlinear interaction problem between control mode and mean flow spreading rate is then given in Secs. III–V. Numerical applications and results are discussed in Secs. VI and VII. The paper concludes with remarks about extensions of the present work in Sec. VIII.

II. Formulation

The general description of the formulation of developing wave-like eddies in growing compressible shear flows was given in Refs. 9 and 10. These authors were concerned with the natural occurrence of coherent structures in a supersonic mixing layer and a supersonic two-dimensional jet. They found that for applications toward explaining the structure of the near jet noise field, coherent structures developing in a known mean flow suffices. For simplicity, they considered a cold mixing layer and jet.

To exploit coherent structures for control of mixing and mean flow development, it is imperative that the nonlinear coupling between the control mode(s) and the mean flow be retained. In addition, in applications we are concerned about the enhancement of mixing between a high-speed, hot jet and a slower, cooler external stream. The development of the description of nonlinear interactions between forced coherent modes in a turbulent shear flow has advanced considerably for the case of an incompressible fluid.[18,21] Because of the complexity of compressible flow, even for a perfect gas, not all of the fluid mechanical nonequilibrium interaction details considered more thoroughly in an incompressible fluid are found desirable for carryover to the compressible situation.

We begin with the partial differential equations governing the flow of compressible fluids; a perfect gas with constant specific heats is assumed. Flow quantities are then represented in terms of the mean flow, coherent modes, and fine-grained turbulence contributions.[16,22–26] Through Reynolds (time) averaging and phase averaging, nonlinearly coupled conservation equations in the physical domain for the mean flow, coherent modes, and the fine-grained turbulence are obtained.

The effect of fine-grained turbulence on both the mean flow and on the coherent structures are represented by eddy viscosity effects, similarly to large eddy simulation, e.g., see Ref. 15, and an earlier formulation of coherent structures in turbulent compressible mixing regions and jets.[8–10] The general partial differential equations are then subjected to approximations of the boundary-layer type and the neglect of molecular transport effects relative to turbulent diffusion. Further simplifications are introduced to the mean flow description by the use of a limited form of the Crocco–Busemann relation between the total enthalpy and the velocity in the mean flow shape assumption process. This assumption can be relaxed with no difficulty by use of an explicit integral equation for the enthalpy. Morkovin's[27] hypothesis is invoked, in which turbulence structure is considered to be unaffected by compressibility and, thus, fine-grained turbulence contributions to the pressure and density fluctuations are neglected. The coherent mode equations are derived in a single-mode form, which can be reinterpreted as that for an ensemble of modes for further extensions of interacting multiple modes if desired.

III. Integral Energy Equations

Cross-stream integration is performed to obtain the integral mean flow kinetic energy and the coherent mode kinetic equation, respectively,

$$\frac{1}{2}\frac{\mathrm{d}}{\mathrm{d}x}\int_0^{+\infty}\bar{\rho}\bar{u}\left(\bar{u}^2-U_1^2\right)\mathrm{d}y+\frac{1}{2}\frac{\mathrm{d}}{\mathrm{d}x}\int_{-\infty}^{0}\bar{\rho}\bar{u}\left(\bar{u}^2-U_2^2\right)\mathrm{d}y$$
$$=-\int_{-\infty}^{+\infty}-\bar{\rho}\overline{u'v'}\frac{\partial\bar{u}}{\partial y}\,\mathrm{d}y-\int_{-\infty}^{+\infty}\bar{\rho}\varepsilon\left(\frac{\partial\bar{u}}{\partial y}\right)^2\mathrm{d}y \tag{1}$$

$$\frac{1}{2}\frac{\mathrm{d}}{\mathrm{d}x}\int_{-\infty}^{+\infty}\bar{\rho}\bar{u}\left(\overline{u'^2+v'^2}\right)\mathrm{d}y=-\int_{-\infty}^{+\infty}\left(\overline{u'\frac{\partial p'}{\partial x}}+\overline{v'\frac{\partial p'}{\partial y}}\right)\mathrm{d}y$$
$$+\int_{-\infty}^{+\infty}-\bar{\rho}\overline{u'v'}\frac{\partial\bar{u}}{\partial y}\,\mathrm{d}y-\int_{-\infty}^{+\infty}\bar{\rho}\varepsilon\left\{\frac{4}{3}\left[\overline{\left(\frac{\partial u'}{\partial x}\right)^2}\right.\right.$$
$$\left.\left.+\overline{\left(\frac{\partial v'}{\partial y}\right)^2}-\overline{\frac{\partial u'}{\partial x}\frac{\partial v'}{\partial y}}\right]+\overline{\left(\frac{\partial u'}{\partial y}+\frac{\partial v'}{\partial x}\right)^2}\right\}\mathrm{d}y \tag{2}$$

The fine-grained turbulence quantities do not appear explicitly, but are reflected in the isotropic, compressible eddy viscosity ε. Following earlier works, e.g., see Ref. 28, ε is related to an incompressible eddy viscosity $\tilde{\varepsilon}$ in the form $\bar{\rho}^2\varepsilon=\rho_r^2\tilde{\varepsilon}$, where ρ_r is a reference density. As with Albers and Lees,[28] in which the reference density is chosen to be on the hot side, the reference density ρ_r is chosen in the present problem to be that for the hot jet or core flow density ρ_1.

The physical interpretation of the integral kinetic energy equations (1) and (2) are straightforward: The left-hand side of Eq. (1) is the mean flow advection of the mean kinetic energy defect; the first and second terms on the right-hand side of Eq. (1) are the energy transfer mechanisms to the coherent mode and to the fine-grained turbulence, respectively. In Eq. (2), the left-hand side is the mean advection of the coherent mode kinetic energy; the right side consists of the work done by the coherent mode pressure gradients, the energy transferred from the mean flow, and energy transfer to the fine-grained turbulence, respectively. The eddy viscosity modeling of the energy transfer effects to the fine-grained turbulence in Eqs. (1) and (2) has relegated these effects to be dissipative, as is the case in large eddy simulation. The direction of energy transfer between the coherent mode and the mean flow is left to the local characteristics of the coherent mode. Equations (1) and (2) will lead to amplitude equations for the coherent mode amplitude and the mean shear flow thickness. Subsidiary relations are needed to close the integral problem. These relations are stated in the following; their detailed role will become clear after the discussion of the shape assumptions.

IV. Subsidiary Relations

The mean flow integral momentum equation is

$$\frac{\mathrm{d}}{\mathrm{d}x}\int_0^{+\infty}\bar{\rho}\bar{u}(\bar{u}-U_1)\,\mathrm{d}y+\frac{\mathrm{d}}{\mathrm{d}x}\int_{-\infty}^{0}\bar{\rho}\bar{u}(\bar{u}-U_2)\,\mathrm{d}y\cong 0 \tag{3}$$

The contributions from the fluctuation part have been neglected, which has a negligible effect on the momentum flux. In the present formulation, Eq. (3) will eventually furnish an algebraic relationship between the local shear layer width and the mean centerline velocity.

The mean total enthalpy is $H = c_p\bar{T} + \bar{u}^2/2$. In the present problem, the initial wall boundary layers are considered to be individually isoenergetic so that the hot jet flow has total enthalpy $H_1 = \text{const}$ and enthalpy of the cooler external stream $H_2 = \text{const}$ for which $H_1 > H_2$. In this case, the total enthalpy profile in the free shear layer is expected to behave monotonically and to be of the mixing-layer type. The local temperature distribution is then obtained from $\bar{T} = (H - \bar{u}^2/2)c_p$.

V. Physical Problem and Shape Assumptions

Application to the unconfined mixing region between two streams of different velocities and different total enthalpies is obtained through the shape assumptions that accompany the integral method. In the following, quantities in the hot jet, with subscript 1, are used to nondimensionalize the basic equations. The Howarth–Doronitsyn transformation is applied to the normal coordinate such that $d\eta = (\bar{\rho}/\rho_1)\,dy/\bar{\delta}$, where η is the new transformed, Blasius-type independent variable and $\bar{\delta}$ is the transformed local shear-layer thickness.

A. Mean Flow Shape and Parameters

A splitter plate initially separates an upper and a lower stream with initial velocity and temperature boundary layers. The mean velocity shape accommodates a wake profile imbedded in a mixing region profile to account for the nonsimilar development from upstream wall boundary-layer effects to that of the similar mixing region profile far downstream.[29] This is an important feature because mixing enhancement for short distances is precisely in the region where upstream wall effects are present. The mean velocity shape assumption consists of the sum of a mixing-layer part and a wake contribution; see the schematic in Fig. 1.

The mixing-layer part of the velocity profile is denoted by subscript m, and the value at the centerline is denoted by subscript cm:

$$\begin{aligned} \bar{u}_m &= u_{\text{cm}} + (1 - u_{\text{cm}})\sin(\pi\eta/2\eta_1), \qquad 0 < \eta < \eta_1 \\ \bar{u}_m &= u_{\text{cm}} + (\beta_u - u_{\text{cm}})\sin(\pi\eta/2\eta_2), \qquad \eta_2 < \eta < 0 \end{aligned} \tag{4}$$

where β_u is the velocity ratio U_2/U_1. The scaling constants $\eta_1 = (1 - u_{\text{cm}})/(1 - \beta_u)$ and $\eta_2 = (\beta_u - u_{\text{cm}})/(1 - \beta_u)$ are obtained by matching the shear stress at $\eta = 0$. They satisfy the relation $\eta_1 - \eta_2 = 1$.

The wake contribution to the mean velocity profile is approximated by the algebraic function for the wake defect,

$$\bar{u}_w = u_{\text{cw}}(\eta - \eta_1)^2(\eta - \eta_2)^2(a\eta + b) \equiv u_{\text{cw}}P \tag{5}$$

The function P is used to denote the algebraic function in Eq. (5) for simplicity. The wake defect profile already satisfies $\bar{u}_w = \bar{u}'_w = 0$ at η_1 and η_2, where the prime denotes differentiation with respect to η. The constants $b = 1/\eta_1^2\eta_2^2$ and $a = 2(\eta_1 + \eta_2)b/\eta_1\eta_2$ are found from the centerline condition $\bar{u}_w = u_{\text{cw}}$ and $\bar{u}'_w = 0$ at $\eta = 0$.

The composite wake–mixing-layer velocity profile then becomes

$$\bar{u}(\eta) = \bar{u}_m(\eta) - \bar{u}_w(\eta) \tag{6}$$

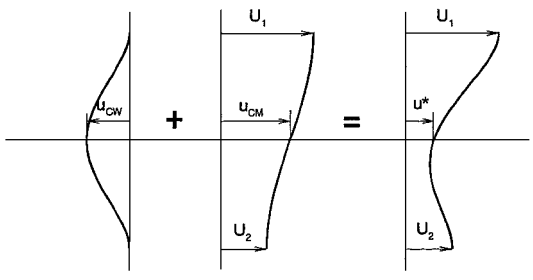

Fig. 1 Mean velocity profiles, schematic.

Following standard nomenclature,[28] the centerline velocity of the composite velocity function is $u^* = u_{\text{cm}} - u_{\text{cw}}$. Far downstream $u^*(\infty)$ should approach that of the fully developed, similarity mixing-layer value $u_s^* = \max(u_{\text{cm}})$. To this end, and to reduce arbitrariness, we assume that $u_{\text{cw}}(x) = r[u_s^* - u^*(x)]$, where r is a proportionality constant to be determined after specifying the initial values $u^*(x_0) = u_0^*$, η_{10} at $x = x_0$. The relationship between $u^*(x)$ and $\bar{\delta}(x)$ and the equilibrium value of $u^*(\infty)$ is addressed in the next section.

B. Relationship Between $u^*(x)$ and $\bar{\delta}(x)$

The mean flow velocity profile (6) contains the two parameters, $u^*(x)$ and $\bar{\delta}(x)$ that are to be jointly solved with the coherent mode problem. At this stage, it is convenient to introduce the shape assumption (6) into the momentum relation (3) to obtain an algebraic relation between the two parameters. To this end, the dimensionless form of Eq. (3) becomes

$$\frac{d}{dx}\bar{\delta}(I_1 - I_2) = 0 \tag{7}$$

where

$$I_1 = \int_0^{+\infty} \bar{u}(1 - \bar{u})\,d\eta, \qquad I_2 = \int_0^{-\infty} \bar{u}(\beta_u - \bar{u})\,d\eta$$

where length scales in the mean flow problem are now normalized by the initial transformed shear flow thicknes $\bar{\delta}_0$. Thus, upon integration, the normalized shear flow thickness is

$$\bar{\delta} = \frac{I_1(x_0) - I_2(x_0)}{I_1 - I_2} \tag{8}$$

The integrals I_1 and I_2, which are evaluated analytically but nevertheless too lengthy to be reproduced here, are functions of u^*. Previous work for the mixing-layer profile alone[9,28] results in a much simpler algebraic relation. Far downstream $\bar{\delta} \to \infty$, $u_{\text{cw}} \to 0$, $u_{\text{cm}} \to u_s^*$, where $u_s^* = 0.587$ for $\beta_u = 0$ and $u_s^* = 0.765$ for $\beta_u = 0.5$.

C. Shape Assumption for Total Enthalpy

The total enthalpy is individually isoenergetic in the hot and in the cooler streams. Therefore, its shape is assumed to follow that of mixing-layer part of the mean velocity profile $\bar{u}_m$:

$$\begin{aligned} \frac{H - H^*}{1 - H^*} &= \frac{\bar{u}_m - u_{\text{cm}}}{1 - u_{\text{cm}}}, \qquad 0 < \eta < \eta_1 \\ \frac{H - H^*}{\beta_H - H^*} &= \frac{\bar{u}_m - u_{\text{cm}}}{\beta_u - u_{\text{cm}}}, \qquad \eta_2 < \eta < 0 \end{aligned} \tag{9}$$

where the total enthalpy ratio is defined as $\beta_H = H_2/H_1$. Matching the normal derivative of H at the centerline gives $H^* = 1 - \eta_1(1 - \beta_H)$. The shape assumption for the total enthalpy is a form of the Bussemann–Crocco relation in that, arguably, the total enthalpy is expected to follow the behavior of the mixing part of the velocity shape assumption expressed in Eq. (4). The dimensionless form of the temperature is then obtained from the definition of the total enthalpy as

$$\bar{T} = \left\{1 + [(\gamma - 1)/2]M_1^2\right\}H - [(\gamma - 1)/2]M_1^2\bar{u}^2 \tag{10}$$

where M_1 is the Mach number of the (hot) core flow. In Eq. (10), H is given by Eq. (9), and $\bar{u}$ is the composite velocity profile given by Eq. (6). The wake contribution to the velocity defect would, thus, contribute to a temperature excess in the initial region. Similarity profiles of the mixing-layer type would be achieved far downstream as the wake defect decays. The total enthalpy assumption here essentially bypasses the necessity of introducing another unknown parameter for the total enthalpy problem. This assumption can always be relaxed through the introduction of an additional integral thermal energy equation to jointly determine a new thermodynamic parameter.[30]

D. Control Wave Mode Shape and Parameters

The coherent mode component is expanded in terms of a nonlinear amplitude, which is to be solved jointly with the mean flow problem, and a cross-stream shape function, which to be given by eigenfunction solutions of a local linear theory at the prevailing local mean flow profiles,[9,10,30]

$$\begin{bmatrix} u' \\ v' \\ p' \\ \rho' \\ T' \end{bmatrix} = A(x) \begin{bmatrix} F \\ \alpha\phi \\ \pi \\ R \\ \theta \end{bmatrix} \exp(-i\omega t) + \text{cc} + \mathcal{O}(A^2) \tag{11}$$

where cc is the complex conjugate. The eigenfunctions F, $\alpha\phi$, π, R, and θ are the shape functions of the corresponding flow quantities on the left-hand side of Eq. (11). They are to be obtained from a local spatial linear theory. As such, the local linear theory dimensionless streamwise length scale and complex wave number α are normalized by the local mean flow length scale $\bar{\delta}$; the local dimensionless time t and real frequency ω are normalized by $\bar{\delta}/U_1$.

It was argued that, for dynamic instability problems in free shear flows, an inviscid local linear theory for the shape functions would be sufficient.[9] In this case, following Lees and Lin,[31] the single equation in terms of the pressure shape function is

$$\pi'' - \frac{2\bar{u}'\pi'}{(\bar{u}-c)} - \alpha^2\bar{T}\left[\bar{T} - M_1^2(\bar{u}-c)^2\right]\pi = 0 \tag{12}$$

with boundary conditions

$$\begin{aligned} &\pi'' - \alpha^2\left[1 - M_1^2(1-c)^2\right]\pi = 0, \qquad \eta \to +\infty \\ &\pi'' - \alpha^2\beta_T\left[\beta_T - M_1^2(\beta_u - c)^2\right]\pi, \qquad \eta \to -\infty \end{aligned} \tag{13}$$

where $\bar{T}$ is now the mean temperature normalized by T_1 and $\beta_T = T_2/T_1$. It is helpful in the classification of flow situations to consider the kinematics of the boundary conditions. Following Lees and Lin[31] (see also Ref. 32), define

$$\begin{aligned} \Omega_+^2 &= \alpha^2\left[1 - M_1^2(1-c)^2\right] \\ \Omega_-^2 &= \alpha^2\beta_T\left[\beta_T - M_1^2(\beta_u - c)^2\right] \end{aligned} \tag{14}$$

so that the relevant phase velocity boundaries are obtained from

$$\Omega_+^2 = 0 \qquad \text{when} \qquad c_+ = 1 - M_1^{-1}$$

$$\Omega_-^2 = 0 \qquad \text{when} \qquad c_- = \beta_u + \beta_T^{\frac{1}{2}} M_1^{-1}$$

The classification[31] is as follows: Subsonic mode, $c_+ < c_r < c_-$; slow supersonic mode, $c_r < c_+$; and fast supersonic mode, $c_r > c_-$, where c_r is the real part of the phase velocity. The slow supersonic mode refers to phase velocity being supersonic with respect to the fast stream, whereas the fast supersonic mode refers to the mode being supersonic with respect to the lower speed stream. For an illustration of the kinematic boundaries of the phase velocity in the present problem, see Fig. 2 of Lee and Liu[33] for the case of $\beta_u = \beta_T = 0.5$. In the vicinity of $M_1 \sim 2$, there appears to be the possibility of all three type of modes present. The actual characteristics of these modes must necessarily follow from the local eigenfunction solutions. Not shown in Fig. 2 of Ref. 33 is the wave mode with wave speed $c_+ = 1 + M_1^{-1}$, for which $c_+ \geq 1$ for finite M_1 and $c_+ \to 1$ as $M_1 \to \infty$. Here we focus attention only on subsonic modes as they are physically expected to be more effective in producing changes in the mean flow in comparison with supersonic modes, the latter being too fast to be in local residence to affect such changes.

We note that, in the local linear theory, lengths are appropriately normalized by local length scales of the mean flow problem. Thus, following standard procedures in the shape assumption for the coherent mode, the local relation $\mathrm{d}A/\mathrm{d}(x/\bar{\delta}) = i\alpha A$ would also be used to evaluate x derivatives of the coherent mode quantities inside the integrals.

E. Physical Quantities to be Solved

The integral kinetic energy equations (1) and (2), upon insertion of the shape functions (6) and (11) and the subsidiary relations (8) and (10), will yield two first-order nonlinear ordinary differential equations for two unknowns: the shear layer thickness ratio $\bar{\delta}/\bar{\delta}_0$ and the coherent mode energy density ratio $|A|^2/|A|_0^2$, where $|A|_0^2$ is the initial energy density. The two nonlinear ordinary differential equations so obtained are

$$\frac{\mathrm{d}}{\mathrm{d}x}(I_M\bar{\delta}) = I_{\text{rs}}|A|^2 + \frac{1}{R_T}I_\Phi \tag{15}$$

$$\frac{\mathrm{d}}{\mathrm{d}x}\left(I_{\text{ke}}|A|^2\right) = \left(I_{\text{rs}} - I_p - \frac{1}{R_T}I_\phi\right)|A|^2 \tag{16}$$

with $\bar{\delta}(x_0) = \bar{\delta}_0$ and $|A(x_0)|^2 = |A|_0^2$ as the upstream initial conditions. The initial frequency parameter for the control coherent mode ω_0 has to be specified. It is important to note that, according to Eq. (15), the shear layer will grow as long as mean flow energy is flowing to the fluctuations, much in the same way as a laminar shear layer grows through viscous dissipation of kinetic energy. This observation, as in the case for incompressible flows,[18] bypasses the need for empirical models used in interpretation of shear-layer growth so prevalent in the literature.

The integrals in Eqs. (15) and (16) follow directly from Eqs. (1) and (2), respectively. The mean flow kinetic energy-defect advection and turbulent dissipation integrals in Eq. (15), I_M and I_Φ, respectively, are independent of frequency. The frequency-dependent integrals, which involve coherent structure quantities, are the coherent mode kinetic energy advection integral I_{ke}, the Reynolds stress-energy conversion integral I_{rs}, the pressure work integral I_p, and the turbulent dissipation integral I_ϕ. The integrals are defined in the Appendix.

The local turbulent Reynolds number, written in terms of dimensionless parameters and incorporating the compressibility transformation $\bar{\rho}^2\varepsilon = \rho_r^2\tilde{\varepsilon}$, becomes $R_T = \bar{\delta}/\rho_r^2 K_\theta\bar{\theta}$, where $\tilde{\varepsilon} = K_\theta\bar{\theta}$ is a dimensionless incompressible eddy viscosity, $K_\theta \approx 0.06$, and $\bar{\theta}$ is the dimensionless, transformed momentum thickness:

$$\bar{\theta} = \int_0^{+\infty} \bar{u}(1-\bar{u})\,\mathrm{d}\eta + \int_{-\infty}^{0} \bar{u}(\beta_u - \bar{u})\,\mathrm{d}\eta = I_1 - I_2$$

The dimensionless reference density, as already discussed, is referenced to the hot core flow, and thus, its value is unity.

VI. Numerical Applications

The integration of Eqs. (15) and (16) is subjected to upstream initial conditions and, thus, forms the basis for a simple open-loop control of the mixing layer. One specifies the coherent mode spectral content (frequencies and wave numbers), initial amplitudes, core flow Mach number, velocity, and temperature ratios.

Numerical applications were performed for a core Mach number $M_1 = 2$ and $\gamma = 1.40$ and various values of $\beta_u = U_2/U_1$, $\beta_T = T_2/T_1$ (and, hence, $\beta_H = H_2/H_1$), and η_{10}, $-\eta_{20}$ to study the effect of velocity and temperature ratios and relative initial shear-layer thicknesses. These values are summarized in Table 1. The β_H ratio follows from the definition of the total enthalpy,

$$\beta_H = \left\{\beta_T + [(\gamma-1)/2]M_1^2\beta_u^2\right\}\left\{1 + [(\gamma-1)/2]M_1^2\right\}^{-1}$$

The convection Mach number[34] is defined as $M_c = M_1(1-\beta_u)(1+\sqrt{\beta_T})^{-1}$ in terms of the present dimensionless mean flow parameters and is included in Table 1 for reference as a mean flow parameter. The initial values of the scaling parameters η_{10}, $-\eta_{20}$ in the mean flow shape assumptions (4–6), which follow from the specified mean

Table 1 $M_1 = 2$, $\gamma = 1.4$

Case	β_u	β_T	β_H	η_{10}	$-\eta_{20}$	M_c	c_-	c_+
1	0.5	0.25	0.25	0.5	0.5	0.59	0.75	0.5
2	0.5	0.25	0.25	0.41	0.59	0.59	0.75	0.5
3	0.5	0.5	0.39	0.5	0.5	0.67	0.85	0.5

flow parameters, are indicative of the relative thicknesses of the initial core flow and of the cooler external stream in the Howarth transformed η plane. It is clear that, in the present context, the convection Mach number itself is insufficient to determine the control characteristics of coherent modes without a thorough discussion of the spectral and amplitude properties.

The control modes chosen here are two-dimensional modes (or axisymmetric modes for initial thin boundary layers compared to the round jet radius) for which the vorticity axis corresponds to that of the mean flow (in the spanwise or circumferential direction). The control parameters studied include variations of the initial coherent mode amplitude and initial dimensionless frequency. To gain insight about the control mode used, Table 1 also shows the fast and slow mode boundaries in terms of the kinematics of the outer boundary conditions for the coherent mode shape assumptions (12–14), an example of which was shown in Fig. 2 of Ref. 33.

VII. Results

The numerical integration was started away from the trailing edge at x_0 for which $u^* = 0.30$ so that the dimensionless streamwise variable is now written as $\xi = x - x_0$, keeping in mind that the normalizing constant is still $\bar{\delta}_0$.

The initial wake region, which is commonly ignored in mixing region studies, has a streamwise lifetime of about $\xi \approx 10 \rightarrow 20$ and, thus, intrudes well into the streamwise region of short mixer-ejectors by a factor of one to three ejector lengths. Thus, in the following, efforts will be directed at studying those coherent modes that could be effective within this short length scale. Detailed results are presented for case 1 in Sec. VII.A; variations from this case to illustrate the effects of changing initial shear layer thickness are presented in Sec. VII.B and that of a warmer external stream in Sec. VII.C.

A. Case 1

1. Shear-Layer Growth Enhancement

The mean shear flow thickness and the coherent mode amplitude for an initial energy density level of 1% are shown in Fig. 2 in the initial mixing region, where the wake component plays a significant role. The initial dimensionless frequency of the control modes ω_0 is used as the parameter. At the top of Fig. 2, the solid line indicates the growth of the turbulent shear flow thickness in absence of explicit coherent mode excitation. The amplitude of the $\omega_0 = 0.4$ mode appears to survive best in the highly damped initial region due to turbulent dissipation. At the end of about $\xi \approx 20$, both the $\omega_0 = 0.4$ and 0.3 modes were able to achieve shear-layer growth of about 20% over that of the undisturbed case, whereas the

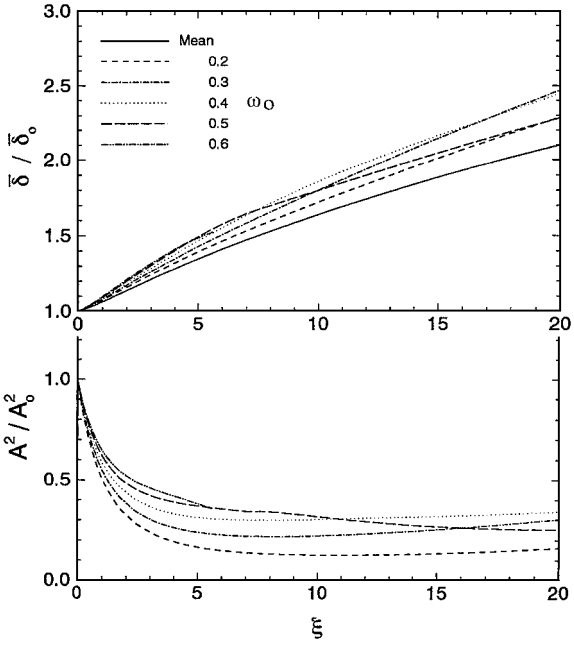

Fig. 2 Case 1, $|A|_0^2 = 0.01$: top, mixing-layer thickness ratio, and bottom, amplitude development.

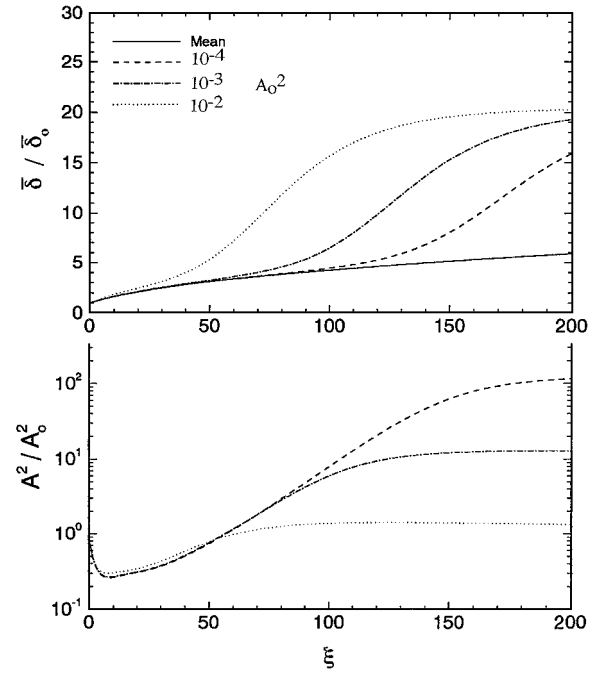

Fig. 3 Case 1, $\omega_0 = 0.4$: top, shear-layer growth, and bottom, amplitude distribution.

$\omega_0 = 0.2$ and 0.5 modes, whose amplitudes decay faster, achieved only about a corresponding 10% increase. Thus, there is an optimal mode $\omega_0 = 0.3$–0.4 in the initial region.

The continued solution beyond $\xi \approx 20$ is shown in Fig. 3 for the $\omega_0 = 0.4$ case at the three different initial amplitudes indicated; the undisturbed case is shown by the solid line. The shear-layer thickness shows a more spectacular early growth for the larger amplitude case, whereas the weak amplitude cases are not efficient enough and their effect is much delayed to the region farther downstream. The amplitude development, which is referenced to the initial amplitude, shows that the weaker initial modes amplify relatively more than the stronger initial modes. This is because the initially stronger modes choke off their own energy supply sooner due to the hastened spreading of the mean flow. Examination of the mean profiles (Sec. VII.A.5) indicates that mean flow similarity is slowly attained beyond $\bar{\delta}/\bar{\delta} \approx 20$ as $u^* \approx 0.75$. Thus, Fig. 3 indicates that the higher amplitude excitation would reach mean flow similarity sooner.

2. Control Mode Characteristics: Subsonic vs Supersonic Mode

The use of local linear theory for the shape functions of the control modes necessitates its interpretation in terms of a fixed initial frequency and the normalization by appropriate local scales of the growing mean flow. When starting from a fixed ω_0, increasing ω thus implies increasing linearly in the transformed shear layer thickness.

We start with the characteristics of the linear theory, in terms of the spatial amplification rate $-\alpha_i$ and the phase velocity c_r, in Figs. 4 and 5 for the subsonic mode ($c_+ < c_r < c_-$) and supersonic slow mode ($c_r < c_+$), respectively. The parameter $u^* = \text{const}$ implies a fixed location in x. Particularly in the region $\omega = 0.3$–0.4, the subsonic modes were able to sustain an $-\alpha_i \cong 0.1$ as u^* progresses downstream, whereas for the supersonic slow modes, $-\alpha_i$ decreases significantly. For the subsonic modes, the initial region supports lower amplification rates, and as the similarity region is approached, the maximum $-\alpha_i$ increases. Thus, subsonic modes are more efficient in sustaining their own growth and are the only modes that are effective as control modes. In the initial region, the subsonic modes accelerate with increasing ω and decelerate with increasing ω as the similarity region is reached, as shown in the bottom panel of Fig. 4. These characteristics are interpreted in terms of a growing shear layer for an initial fixed-frequency parameter in the following.

In the local linear theory, $-\alpha_i$ is made dimensionless by the local shear-layer thickness. The interpretation of the linear theory in terms

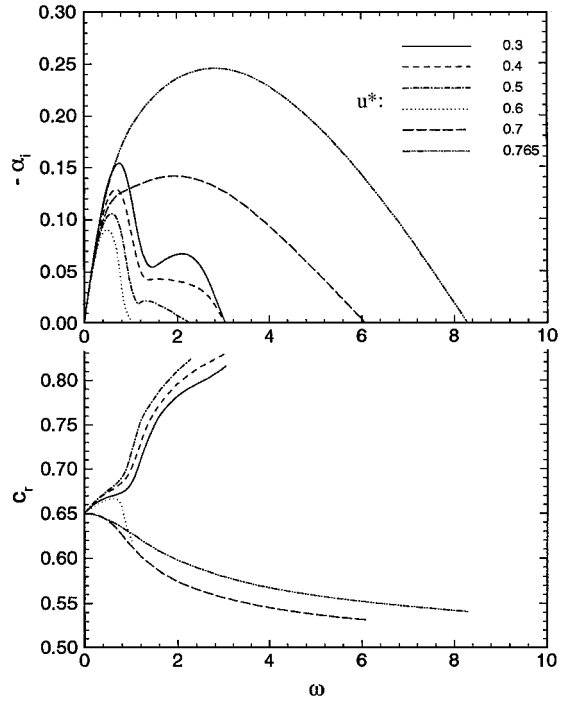

Fig. 4 Linear theory characteristics; subsonic mode, case 1: top, amplification rate, and bottom, phase velocity.

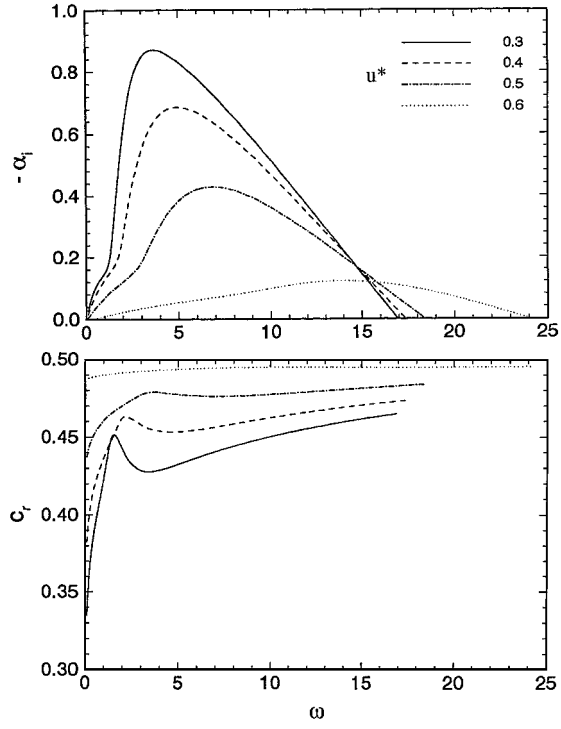

Fig. 5 Linear theory characteristics; slow supersonic mode, case 1: top, amplification rate, and bottom, phase velocity.

of developing flows is shown in Fig. 6 for the subsonic mode, where the amplification rate and phase velocity are plotted as function of the shear-layer thickness (which is like x), with the initial frequency as a parameter. The linear amplification rate does not play an explicit role in the nonlinear, integral theory; nevertheless, it gives an indication of the control modes to chose. Using the top panel of Fig. 6, one then choses an initially most amplified mode, which decays the least as the flow develops. This appears to be satisfied by the $\omega_0 = 0.3$–0.4 modes. The bottom panel of Fig. 6 indicates how the phase velocity would develop downstream for different initial frequencies; the $\omega_0 = 0.3$–0.4 modes eventually slow with increas-

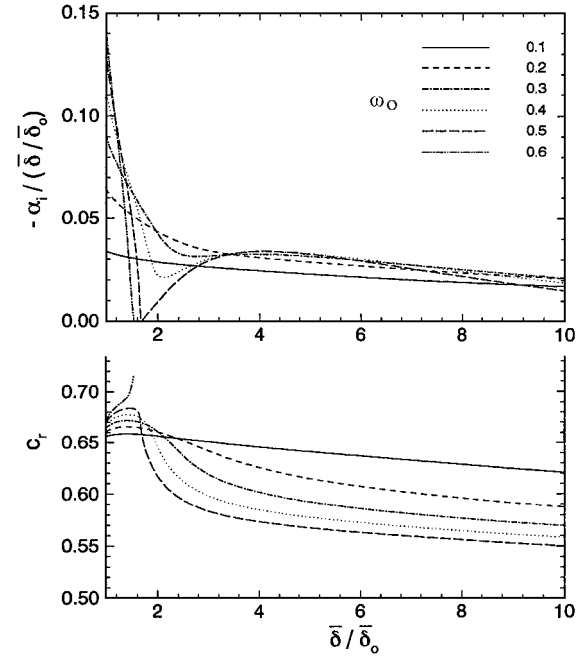

Fig. 6 Interpretation of linear theory characteristics for growing shear layer; case 1: top, amplification rate, and bottom, phase velocity.

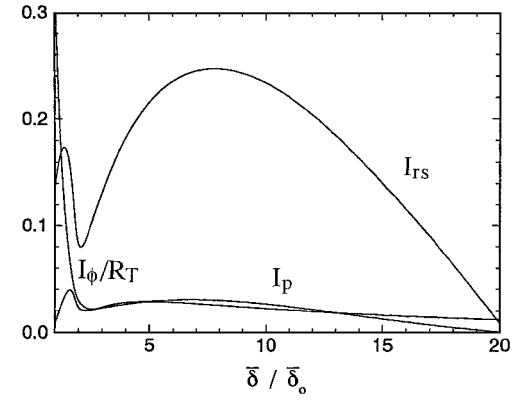

Fig. 7 Interaction integrals; case 1, $\omega_0 = 0.4$.

ing downstream distance. The values of the phase velocities near the similarity region here appear to be in the vicinity of those obtained by Sandham and Reynolds[35] in the linear theory for a computed mixing-layer profile. Although the disturbance effect on growth of the mixing-layer thickness is a mean flow problem associated with the wave envelop A, as shown in Eq. (15), one can perhaps explain physically through wave kinematics that the slower, amplified waves are more efficient extractors of energy from the mean flow (certainly this is true compared to supersonic waves) due to their longer residence time for interaction.

3. *Energy Balancing Mechanisms*

The growth or decay of the shear-layer thickness and the control mode amplitude squared (or energy density) is clearly indicated by Eqs. (15) and (16), in which the interaction integrals play a significant role. Figure 7 shows the interaction integrals as a function of the shear-layer thickness for the subsonic mode. These integrals are tabulated as functions of the shear-layer thickness ratio before solving the x-evolution problem; those integrals that involve the coherent mode would be dependent on the initial frequency parameter. The Reynolds stress energy conversion integral I_{rs} is influenced strongly by the wake-defect region, as indicated by the small initial peak. As the flow evolves toward the similar mixing-region profile, a larger, second peak in I_{rs} is traversed. The amplification rates from the local linear theory, which is no longer effective in the nonlinear integral energy balance, nevertheless give some indication of the character

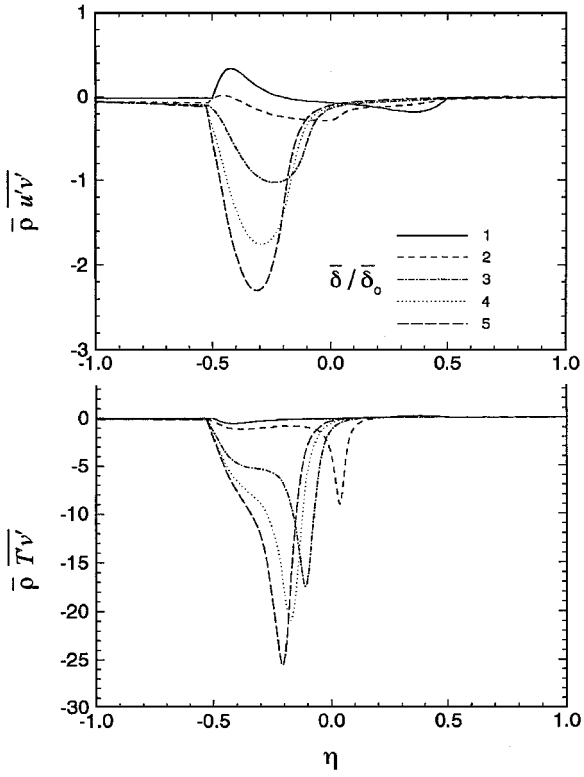

Fig. 8 Negative of Reynolds shear stress and normal heat flux; case 1.

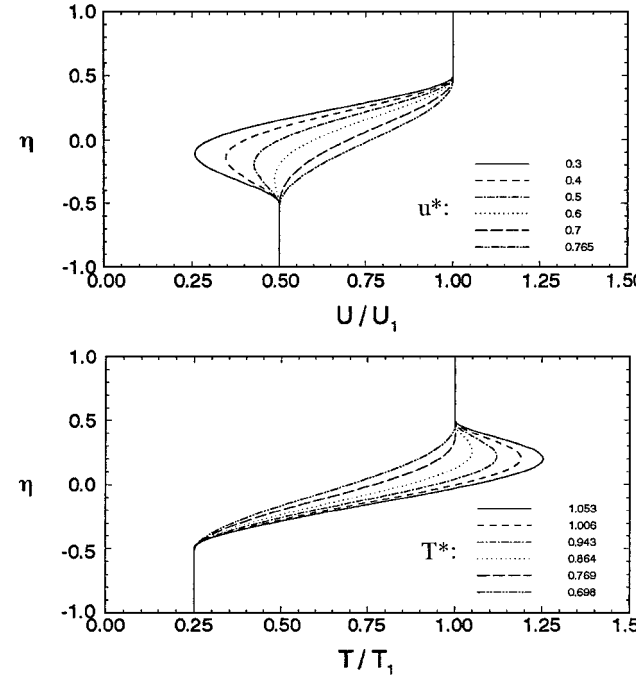

Fig. 9 Case 1: top, mean velocity profiles, and bottom, mean temperature profiles as function of the transformed similarity variable.

of the linear shape functions that is evolving with increasing shear-layer thickness (see Fig. 6). The turbulent dissipation integral for the coherent mode I_ϕ/R_T overwhelms the initial shear-layer energy balance mechanisms, and this accounts for the decay of coherent amplitude in the initial mixing region (see Figs. 2 and 3). Eventually I_ϕ/R_T decays to as low a level as the work done by the coherent mode pressure gradients I_p.

4. Control Mode Reynolds Stress and Heat Flux

The Reynolds shear stress and eddy heat flux for the case 1 subsonic mode are shown in Fig. 8. They both change signs across the shear layer but not necessarily in unison with the changes in sign of the respective velocity and temperature gradients. However, the net effect of the work done against the Reynolds shear stress by the mean rate of strain consistently gives a net positive value to the energy conversion integral I_{rs} (Fig. 7). The conversion mechanism for $\overline{T'^2}$, which was not needed here, was not computed.

5. Mean Velocity and Temperature Profiles

The velocity and temperature profiles in the transformed plane are shown in Fig. 9, with u^* as parameter. A similar profile is reached when $u^* = 0.765$ in this case. The evolution of the disturbed mean velocity and temperature profiles in the physical plane, omitted here, is shown in Fig. 11 of Ref. 33. The velocity leaves the upstream nozzle exit with a wake-type velocity defect as already discussed; the temperature leaves an upstream insulated wall. The wake effect appears to have decayed toward the mixing-layer profile in the region $\xi \approx 10$–20. In the physical plane, it is difficult to see the difference from the undisturbed mean flow profiles; however, comparisons of the shear-layer growth in Figs. 2 and 3 are much clearer indications of the differences between disturbed and undisturbed mean flows.

The evolution of centerline, starred, values of the velocity, temperature, and total enthalpy, which are not reproduced here, are shown in Fig. 12 of Ref. 33 as a function of $\bar{\delta}/\bar{\delta}_0$; far downstream as $\bar{\delta}/\bar{\delta}_0 \to \infty$, the similarity values are reached for which $u^* = 0.765$, $T^* = 0.673$, and $H^* = 0.6475$. However, similarity is essentially slowly attained beyond $\bar{\delta}/\bar{\delta}_0 \approx 20$ as $u^* \approx 0.75$. The relation of the physical shear-layer thickness ratio as a function of the transformed ratio is also shown in Fig. 12 of Ref. 33, obtained with the use of the local temperature profiles in inverting the Howarth transformation; the slope of this line has a value of $\frac{3}{4}$.

B. Case 2: Effect of Initial Shear-Layer Thicknesses

In case 2, the initial conditions are identical to case 1 except that the core flow shear initial shear-layer thickness is slightly less than that of the external flow ($\eta_{10} = 0.41$ and $-\eta_{20} = 0.59$; see Table 1). The linear theory characteristics are shown in Fig. 13 of Ref. 33, in contrast to the equal initial shear-layer thickness case shown in Fig. 4 ($\eta_{10} = -\eta_{20} = 0.50$). Whereas the mode characteristics for larger values of u^* remain almost the same, the initial, smaller u^* mode characteristics are shifted toward higher amplification rates; qualitative and quantitative changes in the phase velocity, which are not shown here, are also contrasted in Fig. 13 of Ref. 33 from those of case 1. Less noticeable changes are associated with the growing shear flow interpretation, shown in Fig. 14 of Ref. 33 (compare with Fig. 6). In case 2, the undisturbed shear-layer thickness is less than that of case 1, as shown in the top of Fig. 10 in this paper. The imposed control modes could, in fact, effect a more significant shear-layer growth; the relative thickness at the end of $\xi \approx 20$ is about 25% for the $\omega_0 = 0.3$ mode. The amplitudes, shown in the bottom panel of Fig. 10, are less damped in the initial region in case 2. In this case, decreasing the core flow initial shear layer thickness has a beneficial role in mixing enhancement.

C. Case 3: Effect of a Warmer External Stream

In case 3 the conditions are similar to case 1 except that the external flow temperature ratio is raised from $\beta_T = 0.25$ to 0.5 (Table 1). Again, the subsonic mode is considered. Significant change in the linear stability characteristics for case 3 is shown in Fig. 16 of Ref. 33. The smaller, upstream u^* gave higher amplification rates than both cases 1 and 2, whereas the phase velocity is qualitatively similar but quantitatively different. The growing shear flow interpretation is shown in Fig. 17 of Ref. 33, with the initial frequency as the parameter. The $\omega_0 = 0.6$ mode appears to have the highest initial amplification; the $\omega_0 = 0.3$ mode, though it has a lower initial amplification, is sustained farther downstream. The phase velocity of the $\omega_0 = 0.6$ mode is accelerating, whereas that of the $\omega_0 = 0.3$ mode is decelerating. In this case, these two modes could give a more rapid spread of the shear flow in the early and later regions, respectively, as indicated on the top figure of Fig. 11. The amplitude of the $\omega_0 = 0.6$ mode is similar to case 2; but the $\omega_0 = 0.3$ mode sustains a higher level than case 2 (Fig. 10).

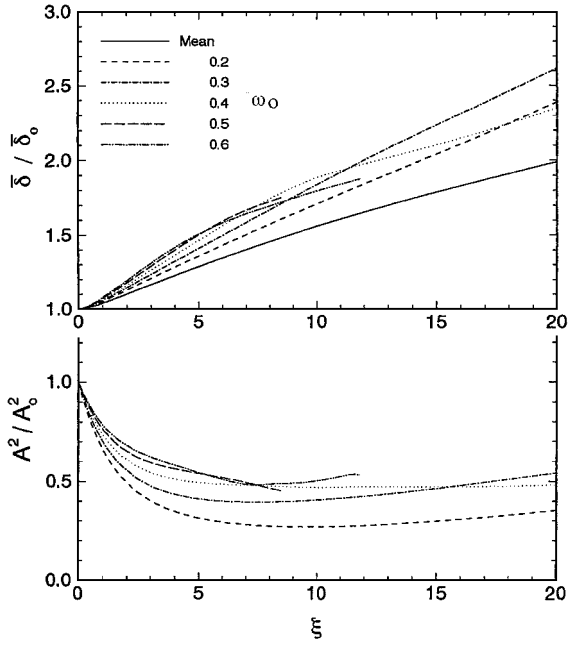

Fig. 10 Case 2, $|A|_0^2 = 0.01$: top, shear-layer growth, and bottom, amplitude development.

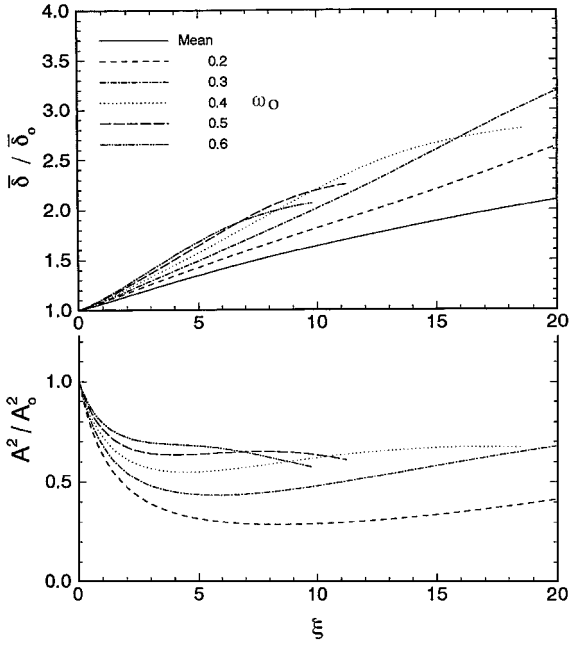

Fig. 11 Case 3, $|A|_0^2 = 0.01$: top, shear-layer growth, and bottom, amplitude development.

VIII. Conclusion

Clearly, the present contribution is meant as a first step in studies of using excited coherent modes to enhance mixing and spreading of compressible shear flows. One foresees the possibility of using interacting oblique waves in generating a mean flow correction component. These obligue waves in turn produce streamwise vorticity for more significant mixing than could be achieved by two-dimensional waves alone.[36,37]

Whereas the paper is concerned with controlling the initial supersonic turbulent mixing region, it is interesting to estimate what effect the initial region-excited coherent modes may have on possible shortening of the potential core of an actual jet. For order-magnitude estimates, we continue to use transformed boundary-layer thickness $\bar{\delta}_0$ as the characteristic length. Referring to Fig. 3, the dimensionless $\xi = x - x_0 \approx x$, which is the physical length x normalized by $\bar{\delta}_0$, can be recast into $(x/D)(D/\bar{\delta}_0)$; for an undisturbed potential core length of about $x/D \approx 10$ and nozzle diameter or width to initial boundary-layer thickness ratio of about $D/\bar{\delta}_0 \approx 20$, then $\xi \approx 200$ (and $\bar{\delta}/\bar{\delta}_0 \approx 6$ according to Fig. 3 for the mean) would correspond to the length of the potential core region. The excited coherent mode moves the location of $\bar{\delta}/\bar{\delta}_0 \approx 6$ to 50% of the length of the potential core length of the undisturbed case ($\xi \approx 100$) for an excitation energy density level of $|A|_0^2 = 10^{-3}$ and to 25% ($\xi \approx 50$) for $|A_0^2| = 10^{-2}$. The experimental decrease of potential core length via coherent structure forcing is well known in low-speed turbulent[38] and laminar jets.[19,20]

The two-dimensional jet problem supports both varicose and sinuous modes; the control problem could be obtained in the present context by extending the weak wave perturbations of Merkine and Liu[10] in a supersonic jet to finite amplitude to modify the mean flow. The incompressible round jet problem has been addressed elsewhere[12,13] for a range of Strouhal frequencies. Multiple high-frequency mode interactions in an incompressible round jet, discussed by Lee and Liu,[39] correspond to similar high-frequency mixing-layer modes discussed in this paper. The mean jet flow problems were analytically represented and parameterized through the unknown jet width (and centerline velocity) and were solved simultaneously with the control mode problem. It is conceivable that the mean flow problem could be represented by experimental or computational fluid dynamics data; however, such data would necessarily have to be similarly parameterized to take advantage of the simplicity of the energy method for developing shear flows in solving the control mode energy with the parameters of the mean flow to be controlled.

The present work, once physically formulated, could produce rapid computations in parameter space to assess the regime of relative importance in mixing enhancement hardware design studies. As such, it is seen to compliment computational studies,[15,16,40,41] which are computational-time intensive and do not necessarily possess the agility for parameter space studies and optimization. The present work is also seen to compliment experimental studies of compressible mixing,[42,43] leading to interpretation of frequency (and wavelength) dependence of observed, convected structures. The external wave system is highly susceptible to misinterpretation if the wave system was generated by convecting, amplifying, and decaying coherent mode structures within the shear flow. Interpretations of such external wave systems is given in Refs. 8, 9, 44, and 45. Although the application here is directed toward the decrease of aerodynamically emitting sound sources by the early destruction of high-velocity and temperature gradients, applications toward mixing problems in combustion[46,47] essentially share the same basic framework as the present study and its extensions.

Appendix: Definition of Interaction Integrals

$$I_M = \frac{1}{2}\int_0^{+\infty} \bar{u}(1-\bar{u}^2)\,\mathrm{d}\eta + \frac{1}{2}\int_{-\infty}^{0} \bar{u}\left(\beta_u - \bar{u}^2\right)\mathrm{d}\eta$$

$$I_\Phi = \int_{-\infty}^{+\infty} \left(\frac{\partial \bar{u}}{\partial \eta}\right)^2 \mathrm{d}\eta$$

$$I_{\mathrm{rs}} = \int_{-\infty}^{+\infty} -(F\tilde{\alpha}\tilde{\phi} + \tilde{F}\alpha\phi)\frac{1}{\bar{T}}\frac{\partial \bar{u}}{\partial \eta}\,\mathrm{d}\eta$$

$$I_{\mathrm{ke}} = \frac{1}{2}\int_{-\infty}^{+\infty} \bar{u}(\overline{u'^2} + \overline{v'^2})I\,\mathrm{d}\eta$$

$$I_p = \frac{1}{\gamma M_1^2}\int_{-\infty}^{+\infty} [i\bar{T}(\alpha\pi\tilde{F} - \tilde{\alpha}\tilde{\pi}F) + (\alpha\phi\tilde{\pi}' + \tilde{\alpha}\tilde{\phi}\pi')]I\,\mathrm{d}\eta$$

$$I_\phi = 2\int_{-\infty}^{+\infty} \left\{\bar{T}^2|\alpha|^2\left(\frac{4}{3}|F|^2 + |\alpha\phi|^2\right) + i\bar{T}\left[(\alpha^2\phi\tilde{F}' - \tilde{\alpha}^2\tilde{\phi}F') + \frac{2}{3}|\alpha|^2(\tilde{F}\phi' - F\tilde{\phi}')\right] + \left(\frac{4}{3}|\alpha|^2|\phi'|^2 + |F'|^2\right)\right\} I\,\mathrm{d}\eta$$

where $I = 1$ (turbulent region) and $I = 0$ (outside).

Acknowledgments

This work is partially supported by NASA Lewis Research Center Grant NSG3-1484 and National Science Foundation Grant INT96-02043. We are particularly grateful for stimulating discussions with J. Abbott, M. Dahl, M. E. Goldstein, R. R. Mankbadi, J. Miles, G. Raman, E. J. Rice, and K. B. M. Q. Zaman, as well as other staff members of the Internal Fluid Mechanics Division and of the Lewis Research Academy.

References

[1]Bishop, K. A., Ffowcs Williams, J. E., and Smith, W., "On the Noise Sources of the Unsuppressed High Speed Jet," *Journal of Fluid Mechanics*, Vol. 50, Pt. 1, Nov. 1971, pp. 21–31.

[2]Lassiter, L. W., and Hubbard, H. H., "The Near Noise Field of Static Jets and Some Model Studies of Devices for Noise Reduction," NACA Rept. 1261, 1956, pp. 213–224.

[3]Mollo-Christensen, E., "Jet Noise and Shear Flow Instability Seen from an Experimenter's Viewpoint," *Journal of Applied Mechanics*, Series E, Vol. 89, March 1967, pp. 1–7.

[4]Potter, R. C., and Jones, J. H., "An Experiment to Locate Acoustic Sources in a High Speed Jet Exhaust Stream," *Journal of the Acoustical Society of America*, Vol. 42, No. 5, 1967, p. 1214 (abstract).

[5]Brown, G. L., and Roshko, A., "The Effect of Density Difference on the Turbulent Mixing Layer," *Conference on Turbulent Shear Flows*, CP-93, AGARD, 1971, p. 23/1.

[6]Brown, G. L., and Roshko, A., "Structure of the Turbulent Mixing Layer," 13th International Congress of Theoretical and Applied Mechanics, Moscow, USSR, Aug. 1972.

[7]Brown, G. L., and Roshko, A., "On Density Effect and Large Structure in Turbulent Mixing Layers," *Journal of Fluid Mechanics*, Vol. 64, Pt. 4, July 1974, pp. 775–816.

[8]Liu, J. T. C., "On Eddy Mach Wave Radiation Source Mechanism in the Jet Noise Problem," AIAA Paper 71-150, Jan. 1971.

[9]Liu, J. T. C., "Developing Large-Scale Wavelike Eddies and the Near Jet Noise Field," *Journal of Fluid Mechanics*, Vol. 62, Pt. 3, Feb. 1974, pp. 437–464.

[10]Merkine, L.-O., and Liu, J. T. C., "On the Development of Noise-Producing Large-Scale Wavelike Eddies in a Plane Turbulent Jet," *Journal of Fluid Mechanics*, Vol. 70, Pt. 2, July 1975, pp. 353–368.

[11]Tam, C. K. W., and Burton, D. E., "Sound Generated by Instability Waves of Supersonic Flows. Part 2. Axisymmetric Jets," *Journal of Fluid Mechanics*, Vol. 138, Jan. 1984, pp. 273–295.

[12]Mankbadi, R. R., and Liu, J. T. C., "A Study of the Interactions Between Large-Scale Coherent Structures and Fine-Grained Turbulence in a Round Jet," *Philosophical Transactions of the Royal Society of London, Series A: Mathematical and Physical Sciences*, Vol. 298, No. 1443, 1981, pp. 541–602.

[13]Mankbadi, R. R., and Liu, J. T. C., "Sound Generated Aerodynamically Revisited: Large-Scale Coherent Structure in a Turbulent Jet as a Source of Sound," *Philosophical Transactions of the Royal Society of London, Series A: Mathematical and Physical Sciences*, Vol. 311, No. 1516, 1984, pp. 183–217.

[14]Mankbadi, R. R., "The Self-Noise from Ordered Structures in a Low Mach Number Jet," *Journal of Applied Mechanics*, Vol. 57, March 1990, pp. 241–246.

[15]Mankbadi, R. R., Hayder, E., and Povinelli, L. A., "The Structure of Supersonic Jet Flow and Its Radiated Sound," *AIAA Journal*, Vol. 32, No. 5, 1994, pp. 897–906.

[16]Bastin, F., Lafour, P., and Candel, S., "Computation of Jet Mixing Noise Due to Coherent Structures in the Plane Jet Case," *Journal of Fluid Mechanics*, Vol. 335, March 1997, pp. 261–304.

[17]Eggers, J. M., "Velocity Profiles and Eddy Viscosity Distributions Downstream of a Mach 2.22 Nozzle Exhausting to Quiescent Air," NACA TN-D-3601, Sept. 1966.

[18]Liu, J. T. C., "Contributions to the Understanding of Large-Scale Coherent Structures in Developing Free Turbulent Flows," *Advances in Applied Mechanics*, Vol. 26, Academic, New York, 1988, pp. 183–309.

[19]Raman, G., and Rice, E. J., "Subharmonic and Fundamental High-Amplitude Excitation of an Axisymmetric Jet," AIAA Paper 89-0993, Jan. 1989.

[20]Raman, G., Rice, E. J. , and Mankbadi, R. R., "Saturation and the Limit of Jet Mixing Enhancement by Single Frequency Plane Wave Excitation: Experiment and Theory," AIAA Paper 88-3613, July 1988.

[21]Mankbadi, R. R., "Dynamics and Control of Coherent Structures in Turbulent Jets," *Applied Mechanics Reviews*, Vol. 45, No. 6, 1992, pp. 219–248.

[22]Hussain, A. K. M. F., and Reynolds, W. C., "The Mechanics of an Organized Wave in Turbulent Shear Flow," *Journal of Fluid Mechanics*, Vol. 41, Pt. 2, April 1970, pp. 241–258.

[23]Kendall, J. M., "The Turbulent Boundary Layer over a Wall with Progressive Surface Waves," *Journal of Fluid Mechanics*, Vol. 41, Pt. 2, April 1970, pp. 259–281.

[24]Liepmann, H. W., "Free Turbulent Flows," *Mécanicque de la turbulence*, Colloques Internationaux du Centre National de la Recherche Scientifique, Centre National de la Recherche Scientifique, Paris, 1962, pp. 211–227.

[25]Phillips, O. M., *The Dynamics of the Upper Ocean*, Cambridge Univ. Press, Cambridge, England, UK, 1966, p. 60.

[26]Townsend, A. A., *The Structure of Turbulent Shear Flow*, 1st ed., Cambridge Univ. Press, Cambridge, England, UK, 1956, pp. 123, 124.

[27]Morkovin, M. V., "Effects of Compressibility on Turbulent Flows," *Mécanicque de la turbulence*, Colloques Internationaux du Centre National de la Recherche Scientifique, Centre National de la Recherche Scientifique, Paris, 1962, pp. 367–380.

[28]Alber, I. E., and Lees, L., "Integral Theory for Supersonic Turbulent Base Flows," *AIAA Journal*, Vol. 6, No. 7, 1968, pp. 1343–1351.

[29]Miau, J. J., "An Experimental Study on the Instability of a Mixing Layer with Laminar Wake as the Initial Condition," Ph.D. Thesis, Div. of Engineering, Brown Univ., Providence, RI, May 1984.

[30]Liu, J. T. C., and Gururaj, P. M., "Finite-Amplitude Instability of the Compressible Laminar Wake. Comparisons with Experiments," *Physics of Fluids*, Vol. 17, No. 3, 1974, pp. 532–543.

[31]Lees, L., and Lin, C. C., "Investigation of the Stability of the Laminar Boundary Layer in a Compressible Fluid," NACA TN-1115, Sept. 1946.

[32]Jackson, T. L., and Grosch, C. E., "Inviscid Spatial Stability of a Compressible Mixing Layer," *Journal of Fluid Mechanics*, Vol. 208, Dec. 1989, pp. 609–637.

[33]Lee, K., and Liu, J. T. C., "Mixing Enhancement in the Initial Region of High Speed Jet Exhaust Flows via Excited Coherent Wave Modes," AIAA Paper 96-0547, Jan. 1996.

[34]Papamoschou, D., and Roshko, A., "The Compressible Turbulent Shear Layer," *Journal of Fluid Mechanics*, Vol. 197, Dec. 1988, pp. 453–477.

[35]Sandham, N. D., and Reynolds, W. C., "Compressible Mixing Layer: Linear Theory and Direct Simulation," *AIAA Journal*, Vol. 28, No. 4, 1990, pp. 618–624.

[36]Cohen, J., and Wygnanski, I., "The Evolution of Instabilities in the Axisymmetric Jet. Part 2. The Flow Resulting from the Interaction Between Two Waves," *Journal of Fluid Mechanics*, Vol. 176, March 1987, pp. 221–235.

[37]Liu, J. T. C., and Lee, K., "Streamwise Vorticity Generation, Mean Flow Modification and Mixing Enhancement by Nonlinear Wave Mode Interactions in an Otherwise Axisymmetric Mean Shear Flow," *Bulletin of the American Physical Society*, Vol. 40, Nov. 1995, p. 1966.

[38]Favre-Marinet, M., and Binder, G., "Structure des Jets pulsants," *Journal de Mecanique*, Vol. 18, No. 2, 1979, pp. 357–394.

[39]Lee, S. S., and Liu, J. T. C., "Multiple-Coherent Mode Interactions in a Developing Round Jet," *Journal of Fluid Mechanics*, Vol. 248, 1993, pp. 383–401.

[40]Lele, S. K., "Direct Numerical Simulation of Compressible Free Shear Flows," AIAA Paper 89-0374, Jan. 1989.

[41]Liou, T.-M., Lien, W.-Y., and Hwang, P. W., "Compressibility Effects and Mixing Enhancement in Turbulent Free Shear Flows," *AIAA Journal*, Vol. 33, No. 12, 1995, pp. 2332–2338.

[42]Papamoschou, D., and Robey, H. F., "Optical Technique for Direct Measurement of Power Spectra in Compressible Turbulence," *Experiments in Fluids*, Vol. 17, No. 1/2, 1994, pp. 10–15.

[43]Papamoschou, D., and Bunyajitradulya, A., "Double-Exposure PLIF Imaging of Compressible Shear Layers," AIAA Paper 95-0513, Jan. 1995.

[44]Tam, C. K. W., "Directional Acoustic Radiation from a Supersonic Jet Generated by Shear Layer Instability," *Journal of Fluid Mechanics*, Vol. 46, Pt. 4, April 1971, pp. 757–768.

[45]Sedel'nikov, T. K., "The Frequency Spectrum of the Noise of a Supersonic Jet," *Physics of Aerodynamic Noise*, NASA Technical Translation F-538, 1969.

[46]Hertsberg, J. R., Carlton, J. D., and Bradley, E., "A Split, Bifurcated Diffusion Flame," *Bulletin of the American Physical Society*, Vol. 40, Nov. 1995, p. 2015.

[47]Smith, L. L., Delabroy, O., Lam, I. T., Majamaki, A. J., Karagozian, A. R., Marble, F. E., and Smith, O. I., "PLIF Measurements of Mixing in a Lobed Injector," Western States Section/Central States/Combustion Inst. Spring Meeting, Paper 95 S-140, March 1995.

S. Glegg
Associate Editor